Isotropic-to-nematic transition in confined liquid crystals: An essentially nonuniversal phenomenon

J. M. Fish and R. L. C. Vink

Institute of Theoretical Physics, Georg-August-Universität Göttingen, Friedrich-Hund-Platz 1, 37077 Göttingen, Germany

Computer simulations are presented of the isotropic-to-nematic transition in a liquid crystal confined between two parallel plates a distance H apart. The plates are neutral and do not impose any anchoring on the particles. Depending on the shape of the pair potential acting between the particles, we find that the transition either changes from first order to continuous at a critical film thickness $H=H_x$, or that the transition remains first order irrespective of H. This demonstrates that the isotropic-to-nematic transition in confined geometry is not characterized by any universality class, but rather that its fate is determined by microscopic details. The resulting capillary phase diagrams can thus assume two topologies: one where the isotropic and nematic branches of the binodal meet at $H=H_x$, and one where they remain separated. For values of H where the transition is strongly first order the shift $\Delta\epsilon$ of the transition temperature is in excellent agreement with the Kelvin equation. Not only is the relation $\Delta\epsilon \propto 1/H$ recovered but also the prefactor of the shift is in quantitative agreement with the independently measured bulk latent heat and interfacial tension.

I. INTRODUCTION

It is generally accepted that the first-order isotropic-to-nematic (IN) transition in liquid crystals confined between two parallel plates becomes continuous when the distance H between the plates becomes small [1–6]. Indeed, many simulations are consistent with this picture [7–11] and show that the first-order IN transition terminates at a critical film thickness H_x. Some of these studies have also provided evidence of a continuous transition taking place when $H < H_x$. Note that as $H \to 0$ the system becomes effectively two dimensional (2D). More recently, a (mathematically rigorous) proof appeared, showing that first-order IN transitions in 2D are also possible [12,13]. Inspired by this proof, computer simulations of liquid crystals in 2D were performed, which indeed uncovered strong first-order IN transitions too [14,15]. Hence, the IN transition in confinement can be continuous, as well as first order. Finally, there is the scenario of no transition occurring at all in thin films [16,17], not even a continuous transition of the Kosterlitz-Thouless (KT) type [18]. Regarding experiments on confined liquid crystals, it has proved difficult to resolve continuous IN transitions in thin films [2,19]. Pronounced coexistence between isotropic and nematic domains is typically observed [19–21], which suggests that a transition does take place and that it is first order.

The qualitatively different manifestations of the IN transition in confinement (continuous, first order, absence) rule out any universality class for this transition. What remains of the IN transition in thin films is determined by microscopic detail. The only regime where some "agreement" may be obtained is in the bulk three-dimensional (3D) limit $H \to \infty$. Here, one usually observes a first-order IN transition, with long-range order in the nematic phase. The transition thus breaks the rotational symmetry of the isotropic phase. At the mean-field level, this implies that the transition must be first order [22]. We emphasize that fluctuations can change this result: even in 3D bulk, a genuine *continuous* IN transition is also possible [22,23]. However, most bulk experiments yield

a first-order IN transition, and so the mean-field approximation appears to be valid in this regime. As the film thickness H decreases, fluctuations become increasingly important, and we expect three scenarios to unfold. In the first and most commonly accepted scenario, the IN transition becomes continuous when the film thickness drops below a critical thickness H_x. In addition, confinement is expected to destroy long-range order in the nematic phase, due to the Mermin-Wagner theorem [24]. Instead, quasilong-range order may result, where the orientational correlations decay as a power law with distance. In the second (lesser known) scenario, the IN transition remains first-order irrespective of the film thickness, i.e., all the way down to $H \to 0$. In the third scenario, evidence for which was recently provided [16,17], the IN transition vanishes completely in the thin-film limit.

Given the three scenarios for the IN transition in confinement, all of which are qualitatively different, it is of fundamental interest to establish which "microscopic detail" is responsible for the scenario that ultimately occurs. The aim of this paper is to identify one possible mechanism, using computer simulations of a generalized Lebwohl-Lasher (LL) model. As it turns out, the generalized LL model is capable to reproduce all three scenarios, by tuning just a single parameter in the Hamiltonian. The effect of this parameter is to make the pair interaction "sharp and narrow," meaning that particles interact when aligned but are otherwise rather indifferent to each other. Depending on this parameter, the crossover with decreasing film thickness from first order to continuous behavior can be eliminated completely and the IN transition remains first-order irrespective of H.

The outline of this paper is as follows. We first introduce the generalized LL model and describe the simulation method. Next, we present simulation data showing one example where the IN transition becomes continuous below a critical film thickness H_x and a second example where the transition remains first-order irrespective of the film thickness. We do not consider the scenario where the transition vanishes below H_x as this has recently been done elsewhere [16,17]. A stringent test of the Kelvin equation, describing the shift of the transition temperature as a function of film

thickness is also included. We end with a discussion and summary in Sec. IV.

II. MODEL AND SIMULATION METHOD

We consider a lattice model similar in spirit to the LL model [25]. To each site i of a 3D lattice, a 3D unit vector $\vec{d}_i$ (spin) is attached, which interacts with its nearest neighbors via

$$E = -\epsilon \sum_{\langle i,j \rangle} |\vec{d}_i \cdot \vec{d}_j|^p, \qquad (1)$$

with exponent p and coupling constant ϵ. In this work we absorb a factor of $1/k_BT$ in the coupling constant, with k_B the Boltzmann constant and T the temperature, and so ϵ plays the role of inverse temperature. The lattice is a $L \times L \times H$ rectangular box, with periodic boundary conditions in the lateral L directions but not in the H direction. The parameter H thus plays the role of the film thickness; the minimum thickness that can be studied in this way equals $H=1$, corresponding to a single lattice layer. This setup is identical to the slab geometry used in earlier simulations of the confined LL model [7]. Note that spins at the walls have a lower number of nearest neighbors, but that the walls are otherwise neutral, i.e., we do not impose any anchoring conditions.

In the original LL model the exponent of Eq. (1) equals $p_{LL}=2$. In the bulk limit $H \to \infty$, a (weak) first-order IN transition is observed [25–29] at $\epsilon_\infty \approx 1.34$ [30]. In the thin-film limit $H=1$ recent simulations indicate the absence of any transition when $p=2$ [16,17]. In this work we consider $p>2$. This modification is expected to enhance first-order phase transitions [31], which may then even survive the limit $H \to 1$ [14,15]. In line with previous work [27,29,32], we analyze Eq. (1) in terms of the histogram

$$P(E,S) \equiv P(E,S|H,L,\epsilon), \qquad (2)$$

defined as the probability to observe a system with energy E and nematic order parameter S in a sample of thickness H, lateral extension L and at inverse temperature ϵ. The distribution is obtained by computer simulations using Wang-Landau [33,34] and transition matrix [35] sampling; additional details pertaining to the present model are provided in Ref. [32]. The nematic order parameter S is defined in the usual way as the maximum eigenvalue of the orientational tensor

$$Q_{\alpha\beta} = \frac{1}{2N} \sum_{i=1}^{N} (3d_{i\alpha}d_{i\beta} - \delta_{\alpha\beta}), \qquad (3)$$

with $d_{i\alpha}$ the α component ($\alpha = x, y, z$) of the orientation $\vec{d}_i$ of the spin at site i, the sum over all $N = HL^2$ lattice sites and $\delta_{\alpha\beta}$ the Kronecker delta. In a perfectly aligned sample it holds that $S=1$, whereas an isotropic sample yields $S \to 0$ in the thermodynamic limit (hence, S defined in this way is an intensive quantity). A final ingredient of this work is the use of finite-size scaling (FSS); needed because we seek thermodynamic limit properties. The thermodynamic limit of a film of thickness H is defined by extending the lateral extension
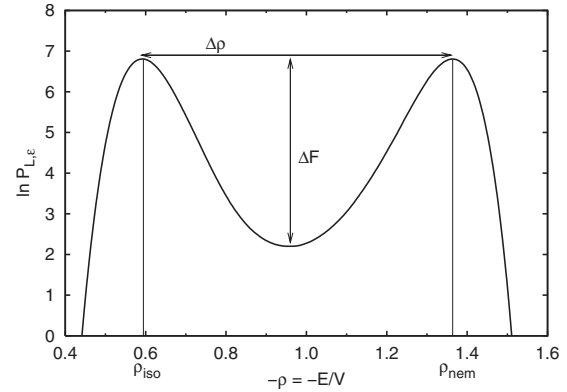

FIG. 1. Logarithm of P using $p=20$ in Eq. (1) with $H=1$ and $L=25$. The value of ϵ has been chosen to give peaks of equal height. The free-energy barrier, labeled ΔF, is given as the difference between the peak maxima straddling the minimum. The distance labeled $\Delta \rho$ corresponds to the latent heat density. The distribution is plotted as a function of the negative energy density such that the left peak corresponds to the isotropic phase and the right peak to the nematic phase.

$L \to \infty$. In the bulk thermodynamic limit, both H and L are taken to infinity.

III. RESULTS

Depending on the exponent p in Eq. (1), we expect the first-order IN transition either to terminate at a critical film thickness H_x or to remain first-order irrespective of H. The case $p=2$, i.e., the original LL model, is an example of the former scenario. In the bulk limit one obtains a first-order transition [25–29], which terminates when the film thickness equals $H_x \sim 8$–16 lattice layers [7]. In the 2D limit $H=1$ no phase transition is observed for $p=2$ [16,17]. We emphasize that the latter finding is not without some controversy, as previous other numerical studies of this system concluded that a phase transition does take place, namely a continuous transition of the KT type (see discussion in Ref. [16]).

A. Crossover scenario

We now consider Eq. (1) using a larger exponent, $p=8$, to demonstrate that also a continuous IN transition is possible in thin films. To determine the order of the transition we use two FSS methods: the first was initially given by Lee and Kosterlitz [36] and is based on the energy distribution $P(E)$, defined as the probability to observe a system with energy E

$$P(E) \equiv \int \int \delta(E-E')P(E',S')dE'dS',$$

with $P(E,S)$ the joint distribution of Eq. (2).

At a first-order transition $P(E)$ becomes bimodal, see Fig. 1 for an example, where the *logarithm* of the distribution is shown. For finite L the bimodal structure persists over a range of ϵ values. As L increases the range becomes smaller and in the thermodynamic limit $L \to \infty$ there is only one ϵ where $P(E)$ is bimodal, then featuring two δ peaks. Hence,
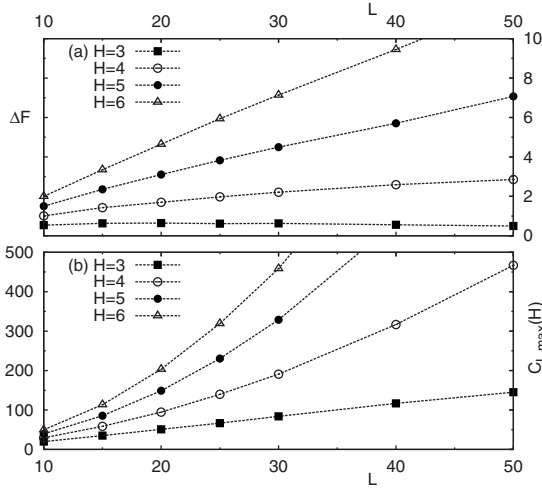
FIG. 2. Evidence of the crossover scenario, whereby the IN transition ceases to be first order below a critical film thickness; the results in this plot refer to $p=8$ in Eq. (1). The free-energy barrier ΔF versus the lateral film extension L is plotted for several values of the film thickness H in (a). For large H the barriers increase linearly with L, consistent with a first-order transition; for smaller H the barrier vanishes with increasing L. The maximum value of the specific heat versus L is plotted in (b), again for several H.

for finite L there is some freedom in choosing ϵ and in Fig. 1 we have tuned ϵ such that the peaks are of equal height.

At a first-order transition the peak height, ΔF in $\ln P(E)$, see the vertical arrow in Fig. 1, corresponds to the free-energy cost of interface formation [37]. We therefore expect $\Delta F \propto L^{d-1}$, with L the lateral extension of the film and $d=2$ (recall that films are effectively two dimensional). To determine the order of the transition, Lee and Kosterlitz [36] proposed to measure ΔF versus L, which should yield a *linear* increase for a film. Results for several values of H are shown in Fig. 2(a). The data clearly indicate that the crossover scenario is taking place: for $H=6$ ΔF increases linearly with L, consistent with a first-order transition. In contrast, for $H=3$ ΔF vanishes for large L, implying the absence of a first-order transition.

To obtain the crossover thickness H_x more accurately we use a second FSS method, based on the specific heat

$$C = (\langle E^2 \rangle - \langle E \rangle^2)/N, \qquad (4)$$

with $N=HL^2$ the number of lattice sites (volume). For given L and H a graph of C versus ϵ reveals a maximum; the value of the maximum defines $C_{L,\text{max}}(H)$. At a first-order transition the maximum scales with the volume of the system, that is $C_{L,\text{max}}(H) \propto N$ [38]. In a film of fixed thickness H this implies $C_{L,\text{max}}(H) \propto L^{\tilde{\alpha}}$ with $\tilde{\alpha}_{1\text{st}}=2$. The result is shown in Fig. 2(b) for several values of the film thickness. For $H=6$ a fit yields $\tilde{\alpha}=2.00$, confirming that the transition is first order. For $H=4$ we obtain $\tilde{\alpha}=1.74$, indicating that a first-order transition is absent. Hence, we conclude that the crossover thickness $H_x=5$. Precisely at H_x a fit yields $\tilde{\alpha}=1.94$, which is still very close to the first-order value. Presumably for $H=5$ the IN transition is weakly first order.

For $H>H_x$, i.e., where the transition is distinctly first order, there is two-phase coexistence at the transition inverse temperature. It seems natural to characterize the phases with the nematic order parameter S. This approach is somewhat dangerous as confinement could destroy long-range nematic order in the thermodynamic limit: $\lim_{L\to\infty} S=0$ irrespective of ϵ. For $H=1$ this follows rigorously from the Mermin-Wagner theorem [24]. The practical problem, affecting both simulations and experiments [39], is that the decay of S with L may be very slow. In fact, finite samples at low temperature typically reveal substantial order, even when the Mermin-Wagner theorem applies [39]. The present simulations are no exception. Shown in Fig. 3(a) is S versus ϵ in the bulk limit $H\to\infty$ for several system sizes L (the bulk simulations were performed on a 3D cube of edge L with periodic boundaries in all directions). A first-order IN transition taking place at $\epsilon \approx 1.52$ [32], where S jumps to a finite value, is clearly seen. More importantly, for ϵ above the transition, S becomes independent of system size, at least on the scale of the graph; the latter is consistent with the formation of long-range nematic order, as expected in 3D. In Fig. 3(b) we show the corresponding result for a film of thickness $H=10$, which is still above the crossover thickness, and so the transition remains first order. The behavior is similar to the bulk case, in the sense that S "jumps" at the transition and for large ϵ it appears to saturate at a finite value independent of the lateral film extension L. Hence, Fig. 3(b) provides no evidence of S decaying to zero in the thermodynamic limit $L\to\infty$, but rather that the film supports long-range nematic order. If S eventually does decay to zero, it is clear that huge system sizes, beyond the reach of any foreseeable simulation, are required to observe it.

To avoid these subtleties, we characterize the coexisting isotropic and nematic phases in the film with their energy densities $\rho_{\text{iso}}(H)$ and $\rho_{\text{nem}}(H)$, respectively. These are simply the peak positions in the energy distribution of Fig. 1. Recall that the latent heat of the transition equals $\mathcal{L}_L(H)=\rho_{\text{nem}}(H)-\rho_{\text{iso}}(H)$, where the subscript is a reminder of finite-size effects in the lateral film extension. The latent heat is related to the specific-heat maximum [38]

$$\mathcal{L}_L(H) = \sqrt{4C_{L,\text{max}}(H)/N}, \qquad (5)$$

and the extrapolation to $L\to\infty$ is performed assuming that $\mathcal{L}_\infty(H)-\mathcal{L}_L(H) \propto 1/N$. The average energy density

$$\rho_L(H) \equiv \frac{\rho_{\text{iso}}(H)+\rho_{\text{nem}}(H)}{2} = \frac{1}{N}\int EP(E)dE,$$

obtained at the specific heat maximum is extrapolated analogously: $\rho_\infty(H)-\rho_L(H) \propto 1/N$. Once $\mathcal{L}_\infty(H)$ and $\rho_\infty(H)$ have been determined, the coexisting energy densities follow. The latter may then be plotted in a capillary phase diagram, see Fig. 4, where the coexistence densities versus inverse film thickness $1/H$ are shown. Since the transition ceases to be first order at the critical thickness H_x the isotropic and nematic branches terminate.

We now consider $H<H_x$. For $H=1$ and $p=2$ in Eq. (1), recent results [16,17] indicate the absence of any phase transition (not even a continuous transition of the KT type). Part
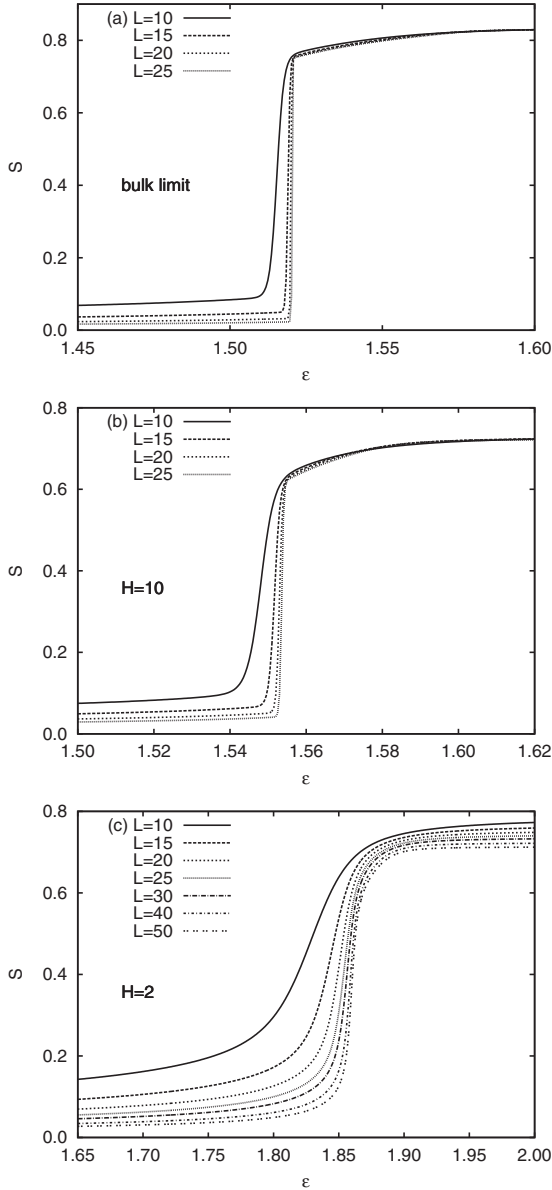
FIG. 3. Variation in the nematic order parameter S versus inverse temperature ϵ using $p=8$ in Eq. (1) for several values of the film thickness H. In (a) we show the bulk result $H \to \infty$, whereas (b) and (c) were obtained in films of finite thickness H. Note that for (a) and (b) the IN transition is first order while it has become continuous in (c).

of the evidence is based on the failure of the Binder cumulant to intersect. At a continuous phase transition the ratio $U_1 = \langle S^2 \rangle / \langle S \rangle^2$ becomes independent of system size [40,41], where S is the nematic order parameter. In simulations, this can be used to locate a continuous transition, by plotting U_1 versus ϵ for several system sizes L. At the transition inverse temperature $\epsilon_\infty(H)$ of the film in the thermodynamic limit the curves for different lateral extensions L are expected to intersect. While for $H=1$ and $p=2$ no intersections are found [17], the result for $p=8$ is radically different, see Fig. 5(a). Shown is U_1 versus ϵ using $H=1$ for several values of L. The curves clearly intersect and so we conclude that a continuous phase transition is taking place. This result strikingly illus-
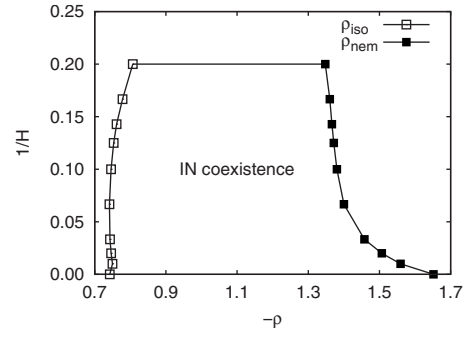

FIG. 4. Capillary phase diagram of Eq. (1) using $p=8$. Shown is the variation in the coexisting phase densities $\rho_{iso}(H)$ and $\rho_{nem}(H)$ with the inverse film thickness $1/H$. The critical inverse thickness is at $1/H_x \sim 0.2$, above which the transition is no longer first order and hence the two branches terminate. In the region between both branches coexistence between isotropic and nematic phases is observed.

trates the nonuniversality of the IN transition: whether a transition occurs for $H=1$ is determined by the exponent p in Eq. (1), i.e., a microscopic detail. Using $p=8$ we have verified that continuous transitions exist for all values of the film thickness $H < H_x$. The results for $H=2$ and $H=4$, where H is approaching H_x, are shown in Figs. 5(b) and 5(c), both of which reveal cumulant intersections.

The fact that the cumulants intersect is a consequence of hyperscaling. At the transition inverse temperature $\epsilon_\infty(H)$ the order parameter decays $\langle S \rangle \propto L^{-\tilde{\beta}}$, while the susceptibility $\chi = N(\langle S^2 \rangle - \langle S \rangle^2)$ diverges $\chi \propto L^{\tilde{\gamma}}$. The exponents $\tilde{\beta}$ and $\tilde{\gamma}$ are connected via the hyperscaling relation

$$\tilde{\gamma} + 2\tilde{\beta} = d, \qquad (6)$$

with spatial dimension $d=2$ for a film. This relation implies that the order parameter and its root-mean-square deviation scale $\propto L^x$ with the same exponent x. Consequently, appropriately constructed cumulant ratios, such as U_1, become independent of L whenever hyperscaling holds. By tuning the inverse temperature ϵ we have determined $\epsilon_\infty(H)$ in our simulations by requiring that the scaling of $\langle S \rangle$ and χ with L conforms to hyperscaling, i.e., we numerically solved Eq. (6). A solution to Eq. (6) for each $H < H_x$ could indeed be found; the resulting estimates of $\epsilon_\infty(H)$, as well as the exponents $\tilde{\beta}$ and $\tilde{\gamma}$, are listed in Table I. As expected, $\epsilon_\infty(H)$ in Table I is close to the cumulant intersections of Fig. 5, the discrepancy being less than 0.1%. Note also that $\epsilon_\infty(H)$ increases with decreasing H. The latter is consistent with the general tendency of confinement to lower phase transition temperatures.

For $H=1$ the system has become 2D and the exponents reflect "pure" values, free from any crossover effects. Note that the exponents for $H=1$ deviate significantly from the XY values $\tilde{\beta}_{XY} = 1/8$ and $\tilde{\gamma}_{XY} = 7/4$ [42], strongly suggesting a different universality class. For $H > 1$, the trend is that $\tilde{\beta} \to 0$, while $\tilde{\gamma} \to 2$. Our interpretation is that, for $1 < H < H_x$, one observes crossover scaling behavior [3], governed by two competing fixed points: one being the first-
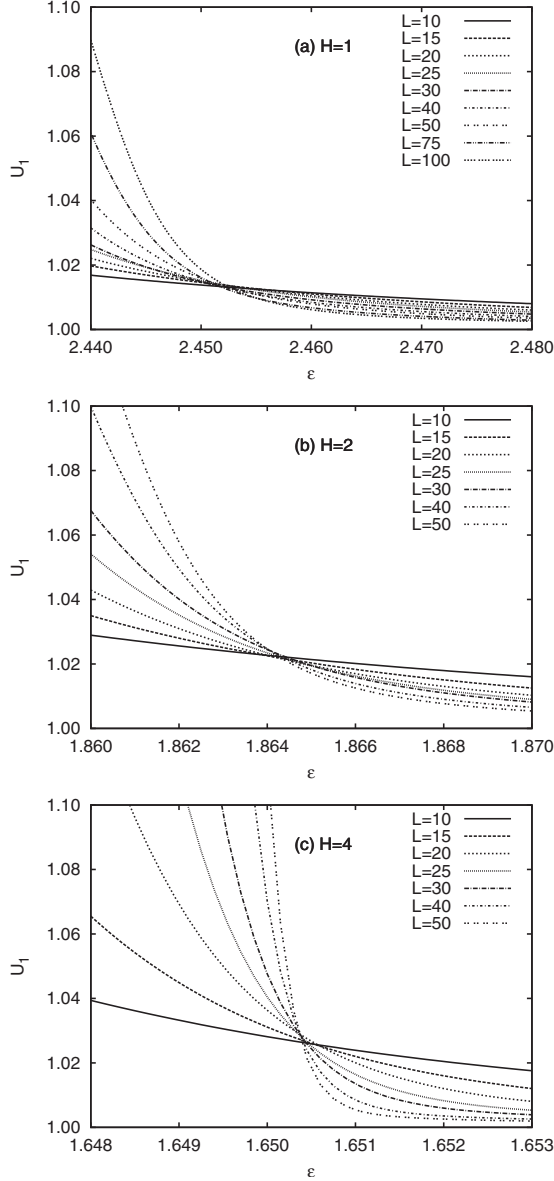
FIG. 5. Cumulant analysis of Eq. (1) using $p=8$. Shown is U_1 versus ϵ using several values of the lateral film extension L, for (a) $H=1$, (b) $H=2$, and (c) $H=4$. The value of ϵ at the cumulant intersection yields the transition inverse temperature $\epsilon_\infty(H)$ of the thermodynamic limit $L \rightarrow \infty$.

order transition at $H=H_x$ and the other being the continuous transition at $H=1$. The exponents for $1 < H < H_x$ are therefore "effective exponents," with values between those of the $H=1$ system, and the "first-order" values $\tilde{\beta}_{1st}=0$ and $\tilde{\gamma}_{1st}=d=2$ [38]. Note that effective exponents do not convey any fundamental information: if we were able to simulate arbitrarily large L values arbitrarily close to the transition inverse temperature, the same exponents as for the $H=1$ system would be found.

The important result to take from this analysis is that for $p=8$ in Eq. (1) and $H < H_x$ a continuous phase transition is found; by enforcing hyperscaling the transition inverse temperature $\epsilon_\infty(H)$ can be quite accurately obtained.

TABLE I. Phase transition properties for $H < H_x$, for the continuous IN transition. Listed is the transition inverse temperature $\epsilon_\infty(H)$, along with the exponents $\tilde{\beta}$ and $\tilde{\gamma}$, versus the film thickness H. The results refer to $p=8$ in Eq. (1).

H	$\epsilon_\infty(H)$	$\tilde{\beta}$	$\tilde{\gamma}$
1	2.450	0.19	1.63
2	1.864	0.17	1.67
3	1.716	0.15	1.71
4	1.650	0.10	1.81

We now consider how the nematic order parameter S depends on ϵ and L; a typical result is shown in Fig. 3(c) where $H=2$ was used. We note that S increases with ϵ and that the slope $dS/d\epsilon$ reaches a maximum close to $\epsilon_\infty(H)$. In contrast to the first-order transitions observed for $H > H_x$, S does not saturate at high ϵ but decreases steadily with increasing L; this behavior is typical for all $H < H_x$. Our simulation data thus suggest the absence of long-range nematic order in the thermodynamic limit when $H < H_x$. This rules out a conventional critical point, since then the order parameter grows as a power law $S \propto t^\beta$, $t>0$, implying $S>0$ in the nematic phase, with distance from the transition

$$t = \epsilon - \epsilon_\infty(H), \qquad (7)$$

and β the critical exponent of the order parameter. It is most likely, therefore, that the continuous transition we observe is a topological transition of the KT type [18].

Consistent with the KT scenario is our previous result of the order parameter decaying $\langle S \rangle \propto L^{-\tilde{\beta}}$ and the susceptibility diverging $\chi \propto L^{\tilde{\gamma}}$, while obeying hyperscaling. For completeness, we provide in Fig. 6 some raw simulation data for the susceptibility. Clearly visible is that χ versus ϵ reveals a maximum, becoming more pronounced for increasing L. In principle, the inverse temperature $\epsilon_{L,\chi}(H)$ where the susceptibility reaches its maximum, in a film of thickness H and lateral extension L, can be extrapolated using

$$\epsilon_{L,\chi}(H) = \epsilon_\infty(H) + \frac{b}{\ln(L/c)^{1/\nu}}, \qquad (8)$$

with nonuniversal constants b and c, and where the exponent ν characterizes the exponential divergence of the correlation length $\xi \propto \exp(bt^\nu)$ for $t<0$, with t given by Eq. (7). For the XY model it holds that $\nu_{XY}=1/2$, but since we did not recover XY exponents in Table I the application of Eq. (8) requires that ν be fitted also, implying a four-parameter fit. We found that such a fitting procedure was numerically difficult to perform, and hence we did not determine $\epsilon_\infty(H)$ in this manner.

Finally, we note that also the specific heat, defined in Eq. (4), is consistent with the KT scenario. Plotted in Fig. 7 is the variation in C with ϵ for several L, using two values of the film thickness. In both cases a maximum is revealed, but for $H=1$ it grows only weakly with L. This is consistent with a negative specific-heat exponent, implying that C remains finite in the thermodynamic limit, which agrees with the KT
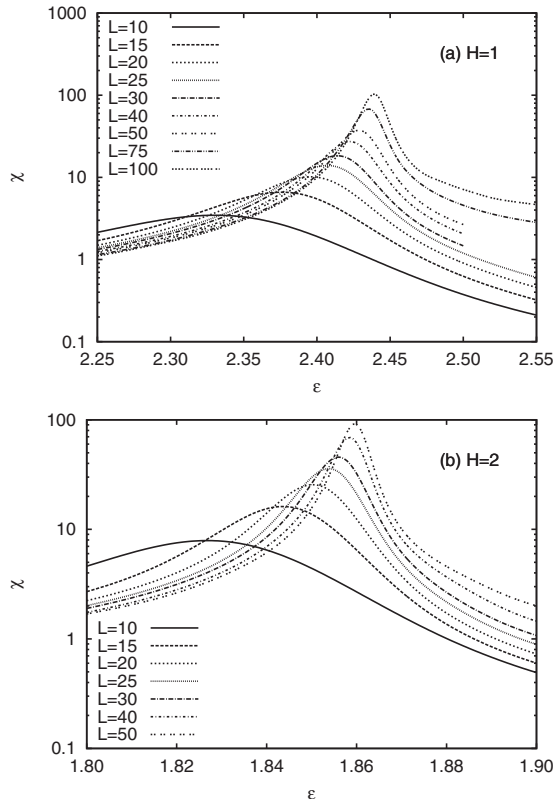
FIG. 6. Variation in the susceptibility χ with inverse temperature ϵ for several values of the lateral film extension L, using film thicknesses (a) $H=1$ and (b) $H=2$. Both of these values $H<H_x$ and so the IN transition is continuous. Note the logarithmic vertical scale. The data were obtained using $p=8$ in Eq. (1).
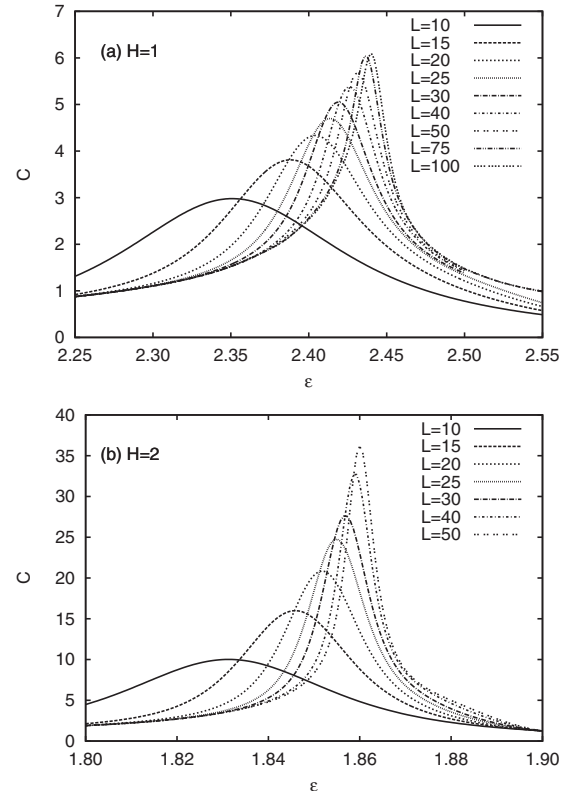

FIG. 7. Variation in the specific heat C with inverse temperature ϵ for several values of the lateral film extension L, using film thicknesses (a) $H=1$ and (b) $H=2$. Both of these values $H<H_x$ and so the IN transition is continuous. The data were obtained using $p=8$ in Eq. (1).

scenario. For $H=2$ we observe that C already grows quite profoundly with L. We again attribute this to the crossover to a first-order transition where, ultimately, the specific-heat maximum should scale $\propto L^{\widetilde{\alpha}}$, with $\widetilde{\alpha}_{1st}=2$, see also Fig. 2(b).

B. First-order transitions

We now consider the IN transition using $p=20$ in Eq. (1). In this case, the transition is strongly first order, even in the thin-film limit. The application of the Lee-Kosterlitz scaling method for $H=1$ is shown in Fig. 8(a), where the linear increase in the barrier ΔF with L is clearly visible. The scaling of the specific-heat maximum also confirms a first-order transition, see Fig. 8(b), showing the expected quadratic dependence of $C_{L,\max}(H)$ on L. Since increasing the film thickness makes the transition more strongly first order, it is clear that for $p=20$ no crossover can occur. In the capillary phase diagram, see Fig. 9, the isotropic and nematic branches of the coexisting energy densities do not terminate, but continue all the way to $H\rightarrow 1$.

C. Kelvin equation

Finally, we study the variation in the inverse transition temperature $\epsilon_{\infty}(H)$ with the film thickness for those cases where the IN transition is first order. We expect $\epsilon_{\infty}(H)$ to fit to the Kelvin equation [4] as
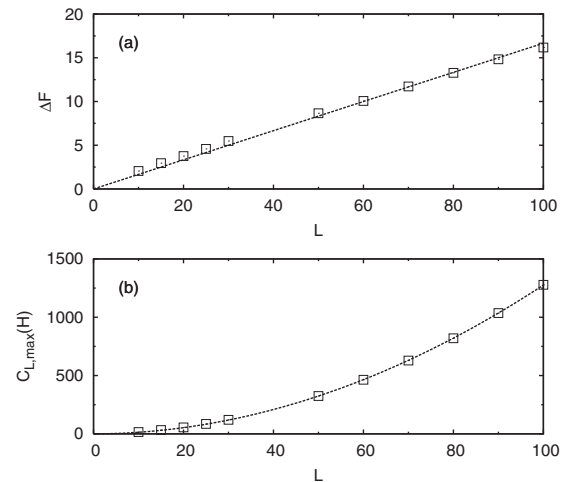

FIG. 8. Scaling analysis of Eq. (1) using $p=20$ and film thickness $H=1$. In (a) we show the variation in the barrier ΔF versus L, while in (b) the specific heat maximum $C_{L,\max}(H)$ versus L is shown. Both these results indicate a first-order phase transition, even though the system is purely 2D. The dashed line in (a) is the result of a linear fit through the origin. The curve in (b) is a fit to the form $C_{L,\max}(H)\propto L^{\widetilde{\alpha}}$; we obtain $\widetilde{\alpha}\approx 1.98$, which is very close to $\widetilde{\alpha}_{1st}=2$ of a first-order phase transition in 2D.
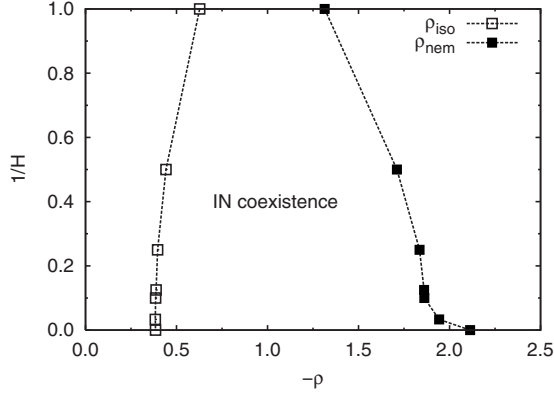
FIG. 9. Capillary phase diagram of Eq. (1) using $p=20$. Shown is the variation in the coexisting energy densities $\rho_{\text{iso}}(H)$ and $\rho_{\text{nem}}(H)$ versus the inverse film thickness $1/H$. In this case no crossover occurs and the IN transition remains first order irrespective of H. The isotropic and nematic branches of the binodal therefore do not terminate, but continue all the way to $H=1$.

$$\Delta\epsilon \equiv 1 - \epsilon_\infty/\epsilon_\infty(H) = \frac{2\gamma_\infty}{\mathcal{L}_\infty H}, \qquad (9)$$

where γ_∞ is the bulk ($H\to\infty$) interfacial tension, ϵ_∞ the bulk IN transition inverse temperature and $\mathcal{L}_\infty$ the bulk latent heat density. In deriving this equation complete wetting is assumed [4]. All quantities that appear in Eq. (9) can, in principle, be extracted from finite-size simulation data with relative ease. For example, $\epsilon_\infty(H)$ at a first-order transition can be obtained from $\epsilon_{L,k}(H)$; the latter is defined as the inverse temperature where the ratio of the peak areas in the energy distribution $P(E)$ equals k. For an optimal value $k=k_{\text{opt}}$, which can be found using trial-and-error, the L dependence in $\epsilon_{L,k}(H)$ becomes negligible and $\epsilon_\infty(H)$ can be accurately obtained [32]. The resulting estimates of the transition inverse temperatures, for both $p=8$ and $p=20$, are provided in Table II, using only values of the film thickness where the transition is first order.

Similar to previously, bulk $H\to\infty$ results are obtained using $L\times L\times L$ systems with periodic boundaries in all directions. The bulk latent heat density $\mathcal{L}_\infty$ is obtained from the specific-heat maximum using Eq. (5) and is once again extrapolated to $L\to\infty$, where now $N=L^3$. The resulting estimate of $\mathcal{L}_\infty$ is also listed in Table II. To obtain the bulk interfacial tension γ_∞ we use the method of Binder [37]. Simulating a large and stretched $L\times L\times D$ system $D>L$ with periodic boundaries in all directions, the logarithm of the energy distribution $P(E)$ reveals a pronounced flat region between the peaks, see Fig. 10. The flat region indicates that the isotropic and nematic phase coexist with only small interactions between the two interfaces. Hence, the average peak height ΔF is related to the bulk interfacial tension

$$\gamma_\infty = \lim_{L\to\infty} \gamma_L, \qquad \gamma_L = \Delta F/(2L^2), \qquad (10)$$

yielding an elegant method of obtaining γ_∞. Provided L is large enough, the result should not depend on the elongation D, but inspection of Fig. 10 reveals this is not quite true,

TABLE II. Dependence of the transition inverse temperature $\epsilon_\infty(H)$ on the film thickness H, for selected values of H where the IN transition is first order. Results are shown for exponents $p=8$ and 20 in Eq. (1). The variation in $\epsilon_\infty(H)$ with H should follow the Kelvin equation, see Eq. (9). The bottom three lines list the bulk ($H\to\infty$) transition inverse temperature ϵ_∞ the bulk latent heat density $\mathcal{L}_\infty$, and the bulk interfacial tension γ_∞, which are required in order to compare to the Kelvin equation.

$p=8$	H	$\epsilon_\infty(H)$	$p=20$	H	$\epsilon_\infty(H)$
	5	1.614		1	2.769
	6	1.593		2	2.175
	7	1.578		4	1.962
	8	1.568		8	1.874
	10	1.555		10	1.858
	15	1.540		30	1.821
	30	1.528			
	50	1.525			
	100	1.522			
	ϵ_∞	1.521		ϵ_∞	1.806
	$\mathcal{L}_\infty$	0.909		$\mathcal{L}_\infty$	1.727
	γ_∞	0.06		γ_∞	0.30

especially for $p=8$. This could indicate that some interaction between the interfaces remains, or that L was not large enough. In any case, using the largest available system size, we obtain $\gamma_\infty\approx0.05$ for $p=8$ and $\gamma_\infty\approx0.29$ for $p=20$ (in units of k_BT per lattice spacing squared). Alternatively, γ_L
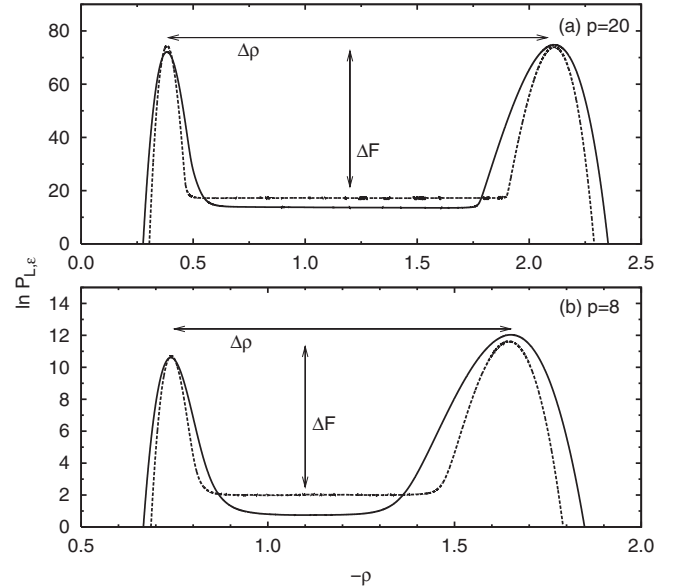

FIG. 10. Plots of $\ln P$ as obtained in completely periodic simulation boxes of size $10\times10\times30$ (solid lines) and $10\times10\times60$ (dashed lines) for (a) $p=20$ and (b) $p=8$. The height of the peaks ΔF is related to the interfacial tension γ_∞ via Eq. (10). The distance $\Delta\rho$ between the peaks is a measure of the latent heat density $\mathcal{L}_\infty$. In these plots ϵ was tuned to yield an approximately horizontal region between the peaks.
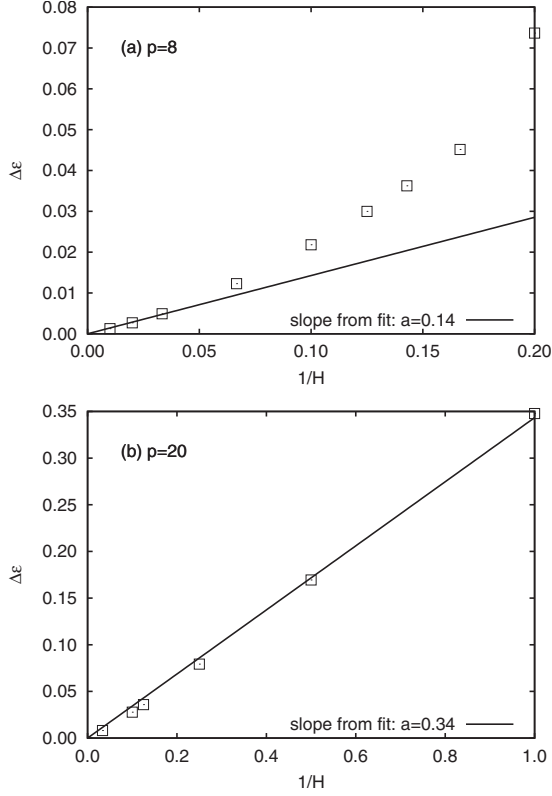
FIG. 11. Test of the Kelvin equation. Plotted is the inverse temperature shift $\Delta\epsilon$ of Eq. (9) versus the inverse film thickness $1/H$, using exponents $p=8$ (a) and $p=20$ (b) in Eq. (1).

can be measured in a cubic periodic system of size L and extrapolation to $L \to \infty$ using

$$\gamma_L = \gamma_\infty + c_1 \ln L/L^2 + c_2/L^2, \qquad (11)$$

with constants c_i, can be attempted [37]. When using this procedure we obtain slightly higher values of the interfacial tension, namely, $\gamma_\infty \approx 0.08$ and $\gamma_\infty \approx 0.31$ for $p=8$ and $p=20$, respectively. Hence, for $p=20$ the estimates for γ_∞ agree reasonably well, whereas for $p=8$ some discrepancy remains. In Table II the average of both estimates is provided.

We now have all quantities needed to put the Kelvin equation to the test, see Eq. (9). Shown in Fig. 11 is $\Delta\epsilon$ versus $1/H$, for both $p=8$ and $p=20$, using only values of H where the transition is first order. Provided the Kelvin equation holds, the resulting plots should be linear. For $p=8$ this is clearly not the case; only in the limit $1/H \to 0$, i.e., where the transition is strongly first-order, is agreement observed. In contrast, using $p=20$ the Kelvin equation holds for all values of the film thickness, including $H=1$. The slope a of the lines in Fig. 11 can be obtained from a fit; following Eq. (9) it is expected that $a=2\gamma_\infty/\mathcal{L}_\infty$, allowing for a stringent quantitative test. For $p=20$ we obtain by fitting $a \approx 0.34$, which is in excellent agreement with $2\gamma_\infty/\mathcal{L}_\infty \approx 0.35$ calculated using the independent estimates of Table II. For $p=8$ the fit yields $a \approx 0.14$, where only the largest three values of H were used. Once again, this is in excellent agreement with $2\gamma_\infty/\mathcal{L}_\infty \approx 0.13$ obtained from Table II.

IV. DISCUSSION AND SUMMARY

In this paper, we have provided results regarding the IN transition in liquid crystals confined between neutral walls. The main conclusion to be taken from this work is that a single universal scenario describing the nature of this transition as function of the film thickness H does not exist. Using a generalized version of the LL model, we have explicitly demonstrated that the first-order IN transition can terminate at a critical thickness H_x, below which it becomes continuous, or that it can stay first-order irrespective of H. The scenario that takes place is determined by a single parameter in the Hamiltonian, namely p in Eq. (1), which sets the "sharpness" of the pair interaction. When the transition is sufficiently strongly first-order excellent agreement with the Kelvin equation is also obtained. In particular, we not only observe the $1/H$ shift of the transition inverse temperature but also the prefactor of the shift is in quantitative agreement with the *independently measured* bulk latent heat and interfacial tension. However, when the IN transition is only weakly first order clear deviations appear and the Kelvin equation significantly underestimates the inverse temperature shift, see Fig. 11(a).

The two different manifestations of the confined IN transition presented in this work yield two distinct phase diagram topologies: one where the isotropic and nematic branches of the binodal terminate at the critical thickness H_x and one where they continue irrespective of H. It is of some interest to compare the resulting phase diagrams to other works. The topology of the $p=8$ phase diagram, see Fig. 4, is commonly encountered in confined colloidal rods and plates [9–11,43]. To facilitate the comparison, the energy density in Fig. 4 should be interpreted as the analog of the particle density in colloidal systems. In agreement with Fig. 4, the first-order IN transition in colloidal systems also terminates at a critical thickness [9–11,43]. It is also interesting to see that the nematic branch of the binodal in Fig. 4 shows rather extreme outward curvature as the bulk limit is approached. Colloidal platelets reveal similar behavior, albeit that here the effect appears in the isotropic branch [43]. In contrast with colloidal systems is the fact that Eq. (1) with $p=8$ in the bulk limit yields a first-order transition that is too strong. Defining the relative strength of the transition as

$$r = \frac{\rho_{nem} - \rho_{iso}}{\rho_{nem} + \rho_{iso}}, \qquad (12)$$

we obtain $r \approx 0.38$ for Eq. (1) with $p=8$, while Onsager's exact solution [44] for infinitely slender rods yields $r \approx 0.12$. This discrepancy can be fixed by using a lower p in Eq. (1). For instance, $p=5$ gives $r \approx 0.15$ [32], which is much closer to Onsager's result. Note that $p=5$ still exceeds the original LL value $p=2$. Indeed, it has been pointed out that the original LL model yields a bulk IN transition that is too weakly first order compared to what is observed in fluids of rods [45].

The second phase diagram topology, where the binodal branches do not terminate in thin films, is obtained for $p=20$ in Eq. (1), see Fig. 9. The resulting phase diagram is of fundamental importance, since it clearly demonstrates that

first-order IN transitions in thin films are also possible and that the crossover to a continuous transition need not necessarily take place. It is interesting that experiments so far have not produced clear evidence of a continuous IN transition in thin films [2,19–21]. This is consistent with a phase diagram topology as shown in Fig. 9. However, it is obvious that the model of Eq. (1) with $p=20$ does not capture the bulk limit correctly, since the bulk IN transition ought to be weak, whereas $p=20$ yields a very strong first-order transition. Clearly, some features are still lacking in Eq. (1), for instance a coupling between the orientational and spatial degrees of freedom of the particles, as well as anchoring effects at the walls. Investigations which incorporate these effects are possible directions for future work.

Finally, using $p=8$ and $H < H_x$ our results show that a genuine continuous IN transition can also take place. Since long-range nematic order is not observed a transition of the KT type [18] is the most likely scenario. This result is interesting because using $p=2$ one finds that Eq. (1) is without any kind of phase transition in the thin-film limit [16,17]. Hence, the nature of the IN transition in thin films is ultimately determined by microscopic details. This means that a single universality class for the IN transition cannot exist. Depending on the details of the interaction, there can be both first order and continuous transitions as well as no transition occurring at all.

[1] P. Sheng, Phys. Rev. Lett. **37**, 1059 (1976).

[2] H. Yokoyama, J. Chem. Soc., Faraday Trans. II **84**, 1023 (1988).

[3] M. M. Telo da Gama and P. Tarazona, Phys. Rev. A **41**, 1149 (1990).

[4] M. M. Telo da Gama, P. Tarazona, M. P. Allen, and R. Evans, Mol. Phys. **71**, 801 (1990).

[5] A. Poniewierski and T. J. Sluckin, Liq. Cryst. **2**, 281 (1987).

[6] P. Sheng, Phys. Rev. A **26**, 1610 (1982).

[7] D. J. Cleaver and M. P. Allen, Mol. Phys. **80**, 253 (1993).

[8] M. C. Lagomarsino, M. Dogterom, and M. Dijkstra, J. Chem. Phys. **119**, 3535 (2003).

[9] M. Dijkstra, R. van Roij, and R. Evans, Phys. Rev. E **63**, 051703 (2001).

[10] M. M. Pineiro, A. Galindo, and A. O. Parry, Soft Matter **3**, 768 (2007).

[11] R. van Roij, M. Dijkstra, and R. Evans, EPL **49**, 350 (2000).

[12] A. C. D. van Enter and S. B. Shlosman, Phys. Rev. Lett. **89**, 285702 (2002).

[13] A. C. D. van Enter, S. Romano, and V. A. Zagrebnov, J. Phys. A **39**, L439 (2006).

[14] R. L. C. Vink, Phys. Rev. Lett. **98**, 217801 (2007).

[15] H. H. Wensink and R. L. C. Vink, J. Phys.: Condens. Matter **19**, 466109 (2007).

[16] R. Paredes V., A. I. Fariñas-Sánchez, and R. Botet, Phys. Rev. E **78**, 051706 (2008).

[17] A. I. Fariñas–Sánchez, R. Botet, B. Berche, and R. Paredes, e-print arXiv:0906.4079.

[18] J. M. Kosterlitz and D. J. Thouless, J. Phys. C **5**, L124 (1972).

[19] M. M. Wittebrood, D. H. Luijendijk, S. Stallinga, T. Rasing, and I. Muševič, Phys. Rev. E **54**, 5232 (1996).

[20] R. Garcia, E. Subashi, and M. Fukuto, Phys. Rev. Lett. **100**, 197801 (2008).

[21] D. van Effenterre, R. Ober, M. P. Valignat, and A. M. Cazabat, Phys. Rev. Lett. **87**, 125701 (2001).

[22] P. G. de Gennes and J. Prost, *The Physics of Liquid Crystals*, 2nd ed. (Oxford University Press, Oxford, 1995).

[23] P. E. Lammert, D. S. Rokhsar, and J. Toner, Phys. Rev. E **52**, 1778 (1995).

[24] N. D. Mermin and H. Wagner, Phys. Rev. Lett. **17**, 1133 (1966).

[25] P. A. Lebwohl and G. Lasher, Phys. Rev. A **6**, 426 (1972).

[26] D. Jayasri, V. S. S. Sastry, and K. P. N. Murthy, Phys. Rev. E **72**, 036702 (2005).

[27] N. V. Priezjev and R. A. Pelcovits, Phys. Rev. E **63**, 062702 (2001).

[28] U. Fabbri and C. Zannoni, Mol. Phys. **58**, 763 (1986).

[29] Z. Zhang, O. G. Mouritsen, and M. J. Zuckermann, Phys. Rev. Lett. **69**, 2803 (1992).

[30] Note that we use the inverse temperature, and also that the definition of the LL model in Eq. (1) differs from the usual one by a factor of 3/2.

[31] S. Romano, Liq. Cryst. **16**, 1015 (1994).

[32] J. M. Fish and R. L. C. Vink, Phys. Rev. B **80**, 014107 (2009).

[33] F. Wang and D. P. Landau, Phys. Rev. Lett. **86**, 2050 (2001).

[34] F. Wang and D. P. Landau, Phys. Rev. E **64**, 056101 (2001).

[35] J.-S. Wang and R. H. Swendsen, J. Stat. Phys. **106**, 245 (2002).

[36] J. Lee and J. M. Kosterlitz, Phys. Rev. Lett. **65**, 137 (1990).

[37] K. Binder, Phys. Rev. A **25**, 1699 (1982).

[38] A. Billoire, R. Lacaze, and A. Morel, Nucl. Phys. B **370**, 773 (1992).

[39] S. T. Bramwell and P. C. W. Holdsworth, Phys. Rev. B **49**, 8811 (1994).

[40] K. Binder, Z. Phys. B **43**, 119 (1981).

[41] K. Binder, Phys. Rev. Lett. **47**, 693 (1981).

[42] J. M. Kosterlitz, J. Phys. C **7**, 1046 (1974).

[43] H. Reich and M. Schmidt, J. Phys.: Condens. Matter **19**, 326103 (2007).

[44] L. Onsager, Ann. N. Y. Acad. Sci. **51**, 627 (1949).

[45] H. Chamati and S. Romano, Phys. Rev. E **77**, 051704 (2008).